American Mineralogist
Vol. 57, pp. 1463–1493 (1972)

COMPOSITION, OPTICAL PROPERTIES, CELL DIMENSIONS, AND THERMAL STABILITY OF SOME HEULANDITE GROUP ZEOLITES

JAMES R. BOLES,[1] *Department of Geology, University of Otago, Dunedin, New Zealand*

ABSTRACT

Cell dimensions, optical, and thermal stability data are given for 14 analyzed heulandites and clinoptilolites, including 7 new analyses from Murihiku Supergroup tuffs, New Zealand. The Murihiku specimens have a wide range of Si/Al ratios (3.0–4.3) and are rich in Ca.

If both loosely and tightly bound water are considered, then 5.7 $\pm$ 0.6 H_2O molecules are co-ordinated about divalent cations; and 3.2 $\pm$ 0.5 molecules about monovalent cations in heulandite group minerals.

Crystals mounted in Lakeside 70 are length fast if Si/Al $\leq$ 3.52 and length slow if Si/Al $\geq$ 3.57. Refractive index is strongly influenced by the types of cations present.

Comparison of calculated cell dimensions indicates that (1) clinoptilolites typically have smaller a, c, and β parameters then heulandites; (2) the area of the ac plane increases with increasing Al or divalent cation substitution; (3) b increases with increasing Mg substitution.

Unit cell dimensions are given for two different contracted phases, phase I and phase B of a dehydrated heulandite from Cape Blomidon, Nova Scotia. The phases appear at temperatures as low as 202°C $\pm$ 3°. For 11 heulandites and clinoptilolite the initial change to phase I occurs at from 213°C to 312°C $\pm$ 3° after heating for 2 hours and cooling for 1 hour.

Three types of thermal stability are recognized in the mineral group. Minerals with a sum of unit cell divalent cations equal to or greater than 1.87 contract after heating. Higher temperatures are required to contract samples with higher Si/Al ratios.

INTRODUCTION

The relationship between heulandite and clinoptilolite has been in dispute for some time. Hey and Bannister (1934) regarded clinoptilolite as isostructural with heulandite and favored the use of the term high-silica heulandite instead of clinoptilolite. Mumpton (1960) and Mason and Sand (1960) regarded the two minerals as distinct species, but did not agree on the means to distinguish them.

Mumpton believed distinction was possible on the basis of Si/Al ratio and he suggested that the higher thermal stability of clinoptilolite provides an easy test for identification. Mason and Sand, on the other hand emphasized cations as the distinguishing feature and stated that heulandites have dominant Ca ions but clinoptilolites have domi-

[1] Present address: Geology Department, University of Wyoming, Laramie, Wyoming 82070.

nant Na and K ions. Furthermore, they suggested that clinoptilolites have a beta index of refraction less than 1.485 but heulandites have a beta index of refraction greater than 1.488.

Although most zeolites of this structural group can be classified using the criteria of both workers, some investigators have reported zeolites with intermediate properties, *e.g.*, Iijima (1961), Hay (1963), Shepard (1961), Brown *et al.* (1970), Alietti (1967; 1972), and Minato and Utada (1970). Anomalous properties were also found by the writer in a study of many altered vitric tuffs from the Murihiku Supergroup of Triassic age, Southland Syncline, New Zealand. The question may be asked: "Do heulandites and clinoptilolites represent distinct compositional groups or do varieties which have *intermediate* compositions exist"? If the latter is true, a redefinition of present terminology is required to classify these intermediate specimens.

This study attempts to clarify the compositional relationship between these zeolites. Furthermore, the relationships between mineral composition and unit cell dimensions, thermal stability, and optical properties were studied to predict the composition by these physical properties. A relatively wide range of Si/Al ratios in the New Zealand samples provided an opportunity to evaluate these properties over a range of compositions.

Sample Preparation

The following sample preparation was used specifically for optical, cell dimension, and thermal stability determinations. After crushing with a TEMA rotary crusher or agate mortar, the $<45\mu$m fraction was obtained by sieving. The powders, except for samples 1 and 6, were repeatedly centrifuged in a bromoform–acetone mixture to obtain the fraction having a density <2.23. This procedure resulted in a zeolite concentrate with <7 percent impurities. Inspection in oils revealed the main impurities to be quartz and phyllosilicate minerals. Centrifuging was not required for samples 1 and 6 as they contain <3 percent impurities. Quartz was used for an internal X-ray standard. Where necessary, a small amount of quartz was added, and the sample was ground for a few minutes to assure mixing of the standard.

Heulandite–Clinoptilolite Chemistry

Table 1 gives heulandite and clinoptilolite analyses for samples from the Murihiku rocks and for specimens from other areas. Zeolites in the Murihiku tuffs were analysed by electron microprobe. Analyses of the other samples are from published wet chemical data of other investigators.

Analytical procedure for EMA analysis

Polished thin sections of each sample were analyzed using a 3-spectrometer ARL electron microprobe analyzer at the Research School of Physical Sciences, Australian National University, Canberra, Australia. Volatilization of light ele-

ments was reduced by using low sample currents of 0.028–0.030 μA at 13.5 kV, and a beam diameter of 10 μm. Silicon, aluminium, and iron were determined simultaneously as were calcium, sodium, and potassium.

A decrease in count rate occurs for sodium with consecutive 4-second counting intervals on the same spot. Potassium and calcium generally show little difference to slight gains with consecutive counting intervals. Silicon and aluminium count rates usually increase slightly with consecutive intervals. The results indicate that the light elements were volatilized. Hence, for each element about 10 spots were analyzed for 4 seconds each, after which another 10 spots were analyzed for 8 seconds each. The counts were averaged for each timed interval and corrected for background and dead time. For samples where obvious volatilization had occurred, the provisional oxide values were extrapolated to zero time. Sodium shows up to 0.30 wt. percent loss of oxide values between 4-second and 8-second counts. Potassium and calcium sometimes show losses of up to 0.15 weight percent. Appropriate gains occur in the provisional oxide values of aluminium and silicon between 4-second and 8-second counts. In some samples, the count rates show opposite trends to what is expected with volatilization, indicating that a slight compositional variation may exist in the sample. Only the more accurate 8-second values were used for calculation in these samples. The compositional variations as inferred from these reverse trends never exceed 2 percent of the amount present. The provisional oxide values were then corrected for atomic number, absorption, and fluorescence.

To check the quality of the extrapolation technique, microprobe analyses were made of a heulandite (sample 1) that was analyzed by wet chemical methods. The corrected microprobe values for SiO_2 and Al_2O_3 are within 1 percent of the amount shown in the wet chemical analyses, and CaO, SrO, Na_2O, K_2O are within 2–6 percent. As only one or two significant figures are reported for the oxides in the west chemical analyses, the agreement is considered satisfactory.

The quality of the EMA analyses can also be checked by the charge balance between the exchangeable cations (including Mg^{2+}) and tetrahedral Al^{3+} substitution. The sum of exchangeable cationic charges in the unit cell should equal the number of R^{3+} cations in the tetrahedral sites in order that the structure be electrically neutral. For samples in Table 1 the charge balance is generally within 0.5 units. Most of the analyses are slightly deficient in exchangeable cations probably as a result of volatilization.

Samples 1, 6, 9, 10 and 12 through 14 are from wet chemical data by other workers; except for number 14, the samples used for this study are reportedly impure portions of the original analyzed specimens. An impure whole rock analysis reported by Ames *et al.* (1958) on the Hector, California tuff is used for sample 14 although the analysis includes some quartz, calcite, and clay minerals. I do not know how closely specimen O.U. 16672 conforms to this analysis. No analyses are available of samples 15 and 16, the former specimen being too fine-grained for EMA analysis even using a beam with a diameter of 10 μm.

Si/Al ratios

Mumpton (1960) proposed a molecular SiO_2/Al_2O_3 ratio of 5.5 to 6.4 for heulandites and 8.5 to 10.5 for clinoptilolites, corresponding to

Si/Al ratios of 2.75–3.25 for heulandites and 4.25–5.25 for clinoptilolites. He also suggested a compositional gap between the two minerals and that clinoptilolite should be classified as a distinct mineral species.

Table 1 shows that all New Zealand samples except numbers 2 and 11 fall within the supposed compositional gap. Samples 6, 9, and 10 also have "intermediate" Si/Al ratios as defined by Mumpton. Similarly Piekarska and Gawel (1954), Hay (1963), Pécsi-Donáth (1966), Alietti (1967) and Brown *et al.* (1969) reported zeolites of this structural group with intermediate Si/Al ratios. Figure 1 is a histogram of Si/Al ratios from published heulandite-clinoptilolite analyses. Also included in Figure 1 are unpublished values for specimens from the Murihiku tuffs which have been analyzed by electron microprobe. Seemingly, Si/Al ratios in the heulandite–clinoptilolite series between 2.75 and 5.25 are possible although most of the heulandites and clinoptilolites probably fall within the two groups defined by Mumpton. Although there seems to be a complete range of Si/Al ratios, zeolites of this structural group with Si/Al ratios of 3.75–4.00 are either rare or rarely analyzed. However, if Si/Al + Fe^{3+} ratios are plotted several more analyses will fall within this interval.

Cation content

Mason and Sand (1960) indicated that heulandites can be distinguished from clinoptilolites on the basis of the ratio of monovalent to divalent cations. They contended that (Na + K) exceeds Ca in clinoptilolites but is less than Ca in heulandites. On this basis, all the New Zealand samples would be classified as heulandites, and the remaining specimens listed in Table 1, except sample 1, would be classified as clinoptilolites.

The New Zealand samples are unusual in that they have low Na/K ratios and are relatively high in Mg. Mg is probably a common impurity in wet chemical analyses of clinoptilolites and heulandites separated from vitric tuffs because of intimately associated phyllosilicate minerals which commonly line the altered glass shards. Electron microprobe analyses should minimize this contamination. Electron microprobe analysis of the phyllosilicate minerals associated with the relict shards in the New Zealand tuffs indicates that total Fe_2O_3 exceeds MgO by a factor of 2 to 5. Low Fe_2O_3 in these samples, except for number 7, indicates that most of the Mg in the analyzed shards of the New Zealand specimens is not related to phyllosilicate impurities. Many of the altered glass shards in the New Zealand tuffs have an abundance of minute reddish brown inclusions which

are thought to be hematite, accounting for at least some of the Fe_2O_3 in the analyses of Table 1.

K–rich specimens with Si/Al ratios > 4.00 have been described from Japan by Minato and Utada (1970). Minato and Utada described sample 10 of Table 1 as a "Ca–clinoptilolite" although on the basis of unit cell contents the specimen is slightly richer in K than Ca.

Although "zeolitic"–type substitution, *i.e.*, $(Na^+, K^+)_2$ for Ca^{2+}, would theoretically permit Na–rich, K–rich, and Ca–rich members of any Si/Al ratio, recorded natural specimens do not show such extensive variation. Conspicuously absent are analyses of natural heulandites with Si/Al < 3.50 and dominantly monovalent cations. The only sample of this type which has been reported is a K–rich heulandite (Si/Al = 3.46) recorded by Alietti (1967).

The reason for the rarity of such variants may be the large number of monovalent cations that would be required to balance the negative charge of the highly aluminous framework. The large number of ions required might create undesirable cation-cation interactions. Nevertheless, such Na (or K) heulandites have been formed from Ca heulandites by means of ion–exchange experiments at temperatures greater than 100°C (Shepard and Starkey, 1966).

H_2O content

The water content for the electron microprobe analyses shown in Table 1 is calculated by difference. Most of these analyses are somewhat low in total water, probably as a result of water loss during probing. Therefore, the unit cell water is not calculated for these samples. The relative increase in the other oxides due to loss of water will not affect the unit cell contents calculated on the basis of 72 oxygen atoms in the anhydrous unit cell.

It is not clear in zeolites which part of the total water content is significant to the structure. I have not attempted to distinguish between loosely and tightly bound water, in part, because Breger *et al.* (1970) have pointed out that determinations of H_2O^+ by conventional methods can give results of doubtful significance in the case of heulandite group minerals. Furthermore, removal of even the loosely bound water results in a structural contraction (Ogawa, 1967; Breger *et al.*, 1970). Most of the more loosely bonded water in a heulandite studied by Merkle and Slaughter (1968) was found to occupy specific sites in the structure.

Breger *et al.* (1970) suggested that the correct amount of tightly bound water in a heulandite and a clinoptilolite which they studied would correspond to 8–9 H_2O molecules per 72 oxygen unit cell. If

TABLE 1: CHEMICAL, OPTICAL, THERMAL STABILITY, AND CELL DIMENSION DATA FOR 16 HEULANDITE GROUP MINERALS

	1	2	3	4	5	6	7	8
SiO_2	56.8	60.61	62.85	63.76	63.56	61.14	64.36	63.01
Al_2O_3	16.6	17.03	15.39	15.52	15.32	14.52	14.30	13.30
Fe_2O_3[b]	tr	0.03	0.38	0.29	0.63	n.d.	1.12	0.67
MgO	tr	0.54	0.77	0.67	0.45	0.28	0.83	1.35
CaO	5.8	6.23	5.24	6.34	7.16	3.60	4.56	3.67
SrO	2.0	0.18	<0.09	<0.09	0.20	n.d.	0.21	<0.09
BaO	n.d.	0.35	<0.17	<0.17	n.d.	n.d.	<0.17	n.d.
Na_2O	1.6	1.07	0.35	0.26	0.12	4.48	0.21	0.24
K_2O	0.8	2.16	2.00	0.33	0.47	0.94	2.40	1.76
H_2O[c]	15.75	11.80	13.02	12.83	12.09	14.16	12.01	16.00
TOTAL	99.44	100.00	100.00	100.00	100.00	99.12	100.00	100.00
Mean refractive index[d]	1.506(3)	1.502(2)	1.500(2)	1.499(1)	1.508(3)	1.487(2)	1.498(1)	1.496(1)
Optical orientation[e]	fast	fast	fast	fast	fast	slow	slow	slow
Unit cell dimension[f]								
a	17.725	17.723	17.703	17.700	17.696	17.670	17.691	17.694
b	17.864	17.915	18.019	17.996	17.944	17.982	18.031	18.054
c	7.427	7.431	7.422	7.426	7.423	7.404	7.412	7.416
β	116°24.2'	116°22.0'	116°21.1'	116°24.9'	116°24.0'	116°23.6'	116°22.7'	116°22.6'
Volume	2,106.5	2,114.3	2,121.6	2,118.7	2,111.3	2,107.4	2,118.4	2,122.7
Thermal stability[g]	H	H	H	H	H	I	I	I
Number of ions on the basis of 72 oxygens								
Si	26.84	27.02	27.29	28.07	27.94	28.00	28.39	28.79
Al	9.25	8.95	8.07	8.05	7.94	7.84	7.43	7.16
Fe^{+3}		0.01	0.13	0.10	0.21		0.37	0.23
Mg		0.36	0.51	0.44	0.29	0.19	0.55	0.92
Ca	2.94	2.98	2.50	2.99	3.37	1.77	2.15	1.81
Sr	0.55	0.05			0.05		0.05	
Ba		0.06						
Na	1.46	0.92	0.30	0.23	0.10	3.98	0.18	0.21
K	0.48	1.23	1.14	0.18	0.26	0.55	1.35	1.03
H_2O	24.82					21.74		
Si/Al	2.91	3.02	3.47	3.49	3.52	3.57	3.82	4.00
2(Ca+Mg+Sr +Ba)+(Na+K)	8.92	9.05	7.46	7.27	7.78	8.45	7.03	6.70

	9	10	11	12	13	14[a]	15	16
SiO_2	63.74	65.17	67.45	64.70	65.10	67.79		
Al_2O_3	13.15	13.38	13.27	12.43	11.06	11.28		
Fe_2O_3[b]	0	1.06	0.31	0.44	1.48	0.86		
MgO	0	0.53	1.03	0.34	1.07	0.40		
CaO	1.37	3.22	3.86	1.26	0.22	0.58	n.d.	n.d.
SrO	n.d.	n.d.	<0.09	n.d.	n.d.	n.d.		
BaO	n.d.	n.d.	<0.17	0.53	n.d.	n.d.		
Na_2O	3.68	1.62	0.26	4.32	5.14	5.96		
K_2O	3.17	2.82	2.26	2.28	2.94	1.07		
H_2O[c]	14.87	11.43	11.56	13.56	12.73	12.06		
TOTAL	99.98	99.39	100.00	99.86	99.74	100.00		
Mean refractive index[d]	1.480(2)	1.487(2)	1.494(2)	1.479(2)	1.477(3)	1.476(2)	1.484(2)	1.500(2)
Optical orientation[e]	slow	slow	slow	slow	slow	slow	slow	fast
Unit cell dimension[f]								
a	17.650	17.683	17.689	17.627	17.635	17.623	17.649	17.718
b	17.917	18.025	18.044	17.955	17.968	17.909	17.902	18.019
c	7.404	7.408	7.408	7.399	7.392	7.395	7.407	7.428
β	116°17.2'	116°24.3'	116°21.2'	116°17.3'	116°18.7'	116°15.3'	116°16.4'	116°23.6'
Volume	2,099.6	2,115.1	2,118.8	2,099.7	2,099.8	2,093.4	2,098.7	2,124.4
Thermal stability[g]	C	I	I	C	C	C	C	H
Number of ions on the basis of 72 oxygens								
Si	29.09	28.78	29.24	29.19	29.27	29.73		
Al	7.07	6.96	6.78	6.61	5.86	5.83		
Fe^{+3}		0.35	0.10	0.15	0.50	0.28		
Mg		0.35	0.67	0.23	0.72	0.26		
Ca	.67	1.52	1.79	0.61	0.11	0.27		
Sr								
Ba								
Na	3.26	1.39	0.23	0.09	4.48	5.07		
K	1.84	1.60	1.25	1.31	1.68	0.60		
H_2O	22.63	16.84		20.40	19.09	17.64		
Si/Al	4.12	4.13	4.31	4.41	5.00	5.10		
2(Ca+Mg+Sr +Ba)+(Na+K)	6.44	6.73	6.40	6.95	7.82	6.73		

[a] *Analyses corrected for CO_2 and equivalent CaO to make calcite.*

[b] *All Fe in electron microprobe analyses assumed to be present as Fe_2O_3.*

[c] *H_2O in electron microprobe analyses determined by difference.*

[d] *Measurements in Na_D light. Mean = $\frac{\alpha + \gamma}{2}$*

[e] *Fast (α') or slow (γ') direction parallel to cleavage or fiber length after mounting in Lakeside 70.*

[f] *Standard error in a, b, c, are less than ±0.002, in β less than ±0.4'*

[g] *Thermal stability refers to changes in X-ray powder diffraction patterns after heating for 15 hours at 450°C.*

C = No change in d-spacings. Minor possible intensity loss

I = Change in d-spacings: however a portion of mineral persists with original d-spacings. Major intensity loss

H = Essentially complete destruction

this small amount of water is the only water which is essential to the structure of the mineral group, then why do naturally occurring specimens show total water contents which consistently vary between 19 and 26 H_2O molecules per 72 oxygen unit cell? For the above reasons, I believe that both loosely and more tightly bound water are important in these minerals. In the discussion to follow the *total* water content as shown by conventional analyses is considered.

Ideal heulandite contains 24 H_2O molecules per unit cell (Hey and Bannister, 1934), and many workers assume that clinoptilolite should have a similar number. However, Mumpton (1960) reported that the molar ratio of H_2O/Al_2O_3 is between 5 and 6 in heulandites and between 6 and 7 in clinoptilolites. Published wet chemical analyses for heulandite and clinoptilolite commonly indicate 23–26 H_2O per unit cell for heulandites and 19–22 H_2O per unit cell for clinoptilolites. Some workers have attributed the low water content of clinoptilolite to loss of weakly held water (Hey and Bannister, 1934; Mason and Sand, 1960). Breger *et al.* (1970) suggested that tightly bound water in heulandite–group zeolites is more firmly held to Ca ions than to Na or K ions. Recent work by Merkle and Slaughter (1968) demonstrated that $5H_2O$ molecules are co-ordinated about each Ca ion in heulandite. Inasmuch as clinoptilolites are usually rich in Na^+–K^+ ions and low in Ca relative to heulandites and as clinoptilolites usually contain

---

1. Heulandite-Ca; OU14989; crystals in basalt cavity; Cape Blomidon, Nova Scotia; Coombs *et al.* (1959) wet chemical analysis by J. A. Ritchie.
2. Heulandite-Ca; OU26044; altered vitric tuff; Taringatura Hills, Southland, New Zealand; EMA analysis by J. R. Boles.
3. Heulandite-Ca; OU26046; altered vitric tuff; Hokonui Hills, Southland, New Zealand; EMA analysis by J. R. Boles.
4. Heulandite-Ca; OU26045; altered vitric tuff; Taringatura Hills, Southland, New Zealand; EMA analysis by J. R. Boles.
5. Si-rich heulandite-Ca; OU26049; altered vitric tuff, Hokonui Hills, Southland, New Zealand, EMA analysis by J. R. Boles.
6. Si-rich heulandite-Na; OU26050, U.S. National Museum catalog number 94512/3; crystals from amygdaloid; Challis, Idaho, Ross and Shannon (1924); wet chemical analysis by E. V. Shannon.
7. Si-rich heulandite-Ca; OU26047; altered vitric tuff; Hokonui Hills, Southland, New Zealand; EMA analysis by J. R. Boles.
8. Si-poor clinoptilolite-Ca; OU26042; altered vitric tuff; Hokonui Hills, Southland, New Zealand; EMA analysis by J. R. Boles.
9. Si-poor clinoptilolite-Na; Y-1 (OU26051); altered tuff from geothermal bore hole; Yellowstone National Park, Wyoming; Honda and Muffler (1970); wet chemical analysis by Toshio Negishi.
10. Si-poor clinoptilolite-K; OU26055; altered vitric tuff; Shizuma, Japan; Minato and Utada (1970); wet chemical analysis.
11. Si-poor clinoptilolite-Ca; OU26043; altered vitric tuff; Taringatura Hills, Southland, New Zealand; EMA analysis by J. R. Boles.
12. Si-poor clinoptilolite-Na; SM-4-4A (OU26052); altered vitric tuff; San Bernardino County, California; Sheppard and Gude (1969); wet chemical analysis by E. S. Daniels.
13. Clinoptilolite-Na; T4-60C (OU26053); altered vitric tuff; Hector, California; Ames *et al.* (1958); wet chemical analysis.
15. Si-poor clinoptilolite -Na or -K[1]; Deep Sea Drilling Project 1-5-3-1 (OU26054); Tuffaceous silty clay sampled at 65–67 feet; Lat. 25°51.5'N Long. 92°11.0'W, Atlantic Ocean.
16. Heulandite-Ca[1]; OU26048; altered vitric tuff; Hokonui Hills, Southland, New Zealand.

[1] Composition estimated from optical, cell dimension, and thermal stability data.

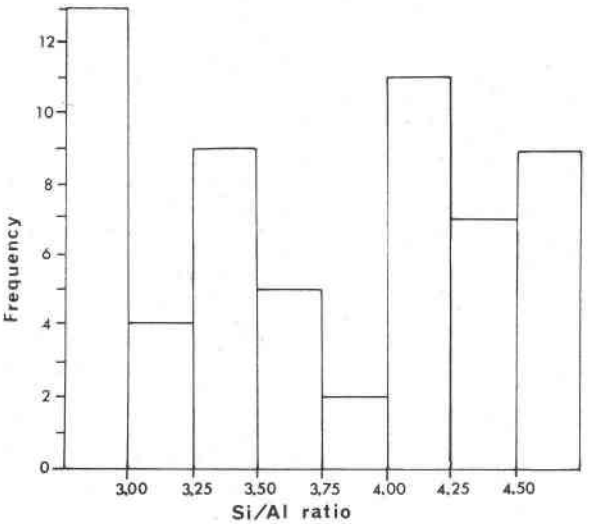

FIG. 1. Frequency histogram of the Si/Al ratios of 60 heulandite group zeolites. Nine unpublished EMA analyses from Murihiku tuffs in addition to those shown in Table 1, have been included.

less *total* water, Na^+–K^+ ions may have fewer total number of water molecules co-ordinated about them than do the Ca^{2+} ions.

To test this hypothesis, unit cell H_2O contents were plotted against $100 \times (Ca + Sr + Mg/Ca + Sr + Mg + Na + K)$ (*i.e.*, percent divalent cations) for wet chemical analyses from the literature (Fig. 2). The plot shows a much closer correlation than a plot of unit cell H_2O vs unit cell Al content, or a plot of Ca + Sr + Mg + Na + K vs unit cell H_2O, and indicates that the *total* water content of the heulandite–clinoptilolite unit cell is a function of the type of cation. Furthermore, total water content increases with the percentage of divalent cations.

An approximation can be made of the number of H_2O molecules co-ordinated about monovalent and divalent cations. If x = number of water molecules about the monovalent cations and y = number of water molecules about the divalent cations, then, for each of the analyses used in Figure 1:

$$\text{Number of } H_2O \text{ per unit cell} = x\,(\Sigma \text{ monovalent cations}) + y\,(\Sigma \text{ divalent cations}).$$

Using a least-squares program and solving all 28 equations for x and y, the H_2O co-ordination number for monovalent cations is 3.2 ± 0.5

and for divalent cations is 5.7 ± 0.6. Grouping all the cations into divalent or monovalent groups is probably a rough approximation as individual cation size and charge/cation radius ratio factors are also probably significant in determining water co-ordination numbers. Nevertheless these calculations confirm that the total water content of heulandites and clinoptilolites is closely related to the proportion of monovalent to divalent cations. Clinoptilolites generally have less total water than heulandites because of high contents of Na^+ and K^+ ions.

The effect of cation type on water content may also be found in other zeolites. Zaporozhteseva (1960) noted that the Ca–zeolite laumontite has a lower H_2O content when the Ca ions are partially replaced by Na or K. Foster (1965) noted that small amounts of Ca tend to increase the H_2O content of the zeolites natrolite, scolecite, and mesolite.

Nomenclature of the Heulandite Mineral Group

At present, there is no general agreement as to the nomenclature for heulandite group minerals (*e.g.*, Mumpton, 1960; Mason and Sand,

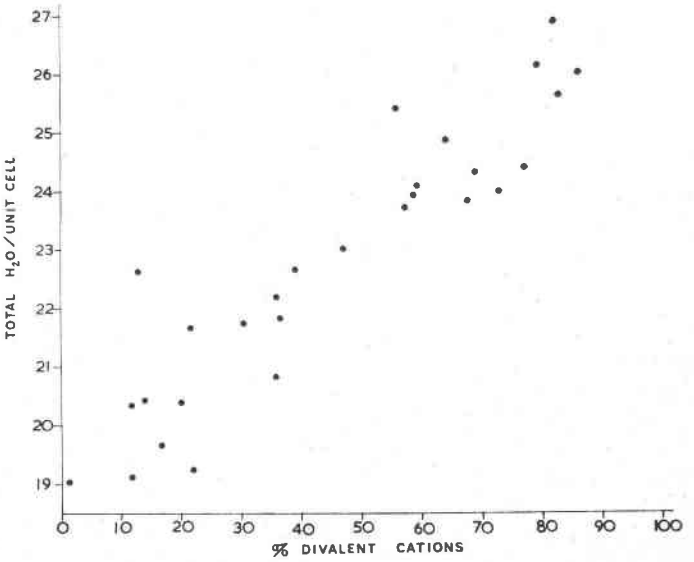

Fig. 2. Plot of unit cell water content (H_2O total) against percent divalent cations ($100 \times [Ca^{2+} + Mg^{2+} + Ba^{2+} + Sr^{2+}/Ca^{2+} + Mg^{2+} + Ba^{2+} + Sr^{2+} + Na^+ + K^+]$) for 28 wet chemically analyzed heulandites.

1960). This problem has become more acute in recent years due to the discovery of minerals with intermediate compositions. For purposes of discussion in this paper, I will use some modifiers to describe members of the heulandite mineral group.

Use of the term heulandite or clinoptilolite should imply some fundamental aspect of their chemistry and not derivative properties such as thermal stability. The silicon and aluminum contents of the tetrahedral framework are a more fundamental property than the predominant type of exchangeable cation, as ion exchange in these zeolites allows substitutions of the type $2Na^{+}$ or $2K^{+} = Ca^{+2}$ (Shepard and Starkey, 1966; Minato and Utada, 1970). Therefore the nomenclature in this paper will follow that proposed by Mumpton (1960) who regarded clinoptilolite as the Si–rich member of the group.

The previous data have shown that no compositional gap exists in terms of Si/Al ratios for members of the heulandite group, thus it is necessary to choose some arbitrary composition to divide the series. As most end–member heulandites have a Si/Al ratio of 2.9–3.0 and end–member clinoptilolites have a ratio of 5.0–5.1, a Si/Al ratio of 4.0 may be used to divide the series. For the purpose of this paper, a member of the series having a Si/Al ratio 4.0 or greater is termed clinoptilolite, and if less than 4.0 is termed heulandite. In terms of unit cell contents, where ideally Si + Al = 36.00, a Si/Al ratio equal to 4.0 corresponds to 28.8 Si atoms. The two groups are further subdivided by the prefix "Si–poor" or "Si–rich". Hence, a Si–rich heulandite would have a Si/Al ratio greater than or equal to 3.5 but less than 4.0, whereas a Si–poor clinoptilolite would have a Si/Al ratio greater than or equal to 4.0 but less than 4.5.

Although the type of cation may not be fundamental to the zeolite framework, evidence presented later in this paper suggests that the type of cation plays an important role in thermal stability and index of refraction, and in unit cell dimensions. Therefore, the dominant cation will be placed as a suffix to each of the above terms, *e.g.*, clinoptilolite–Ca. Examples of the application of these terms to mineral analyses is shown in the explanation to Table 1.

Optical Properties

Index of refraction

Mason and Sand (1960) reported that heulandites have an index of refraction β greater than 1.488 and clinoptilolites have β less than 1.485. Some workers have reported minerals which have β intermediate to this: *e.g.*, Ross and Shannon (1924), Shepard (1961), Hay (1963),

and Brown *et al.* (1969). Before indices of refraction, n, can be used as a means of identifying a mineral as "heulandite" or "clinoptilolite", it is important to evaluate what it means in terms of composition.

Mason and Sand (1960) suggested that heulandite–clinoptilolite n's are a function of both Si/Al ratio and cations. Shepard and Starkey (1966) confirmed that n is in part a function of type of cation substitution as they noted an increase in n when Ca is substituted for Na–K in a clinoptilolite. The New Zealand samples have "heulandite" indices of refraction as defined by Mason and Sand (1960), even though the Si/Al ratio of these samples is 3.02–4.31. The narrow range in mean n of these specimens must be attributed to their high divalent/monovalent cation ratio, and possibly to the higher water content generally associated with divalent cation substitution.

Si/Al ratios are also important in determining the n of heulandite–clinoptilolite. In comparing samples from Table 1 which have similar proportions of divalent/monovalent cations but which differ in Si/Al ratio (*e.g.*, samples 8 vs 11 and 3 vs 7), the effect of Si/Al ratio by itself on index of refraction can be estimated. In these cases, a difference in Si/Al ratio of about 0.3 results in a difference in mean n of about 0.002.

Figure 3 is a plot of Si/Al ratio and dominant cation against mean index of refraction for 41 heulandite group zeolites. Included in the plot are unpublished data on a Si–poor clinoptilolite ($Si/Al + Fe^{3+} = 4.03$) from Wikieup, Arizona, which contains dominantly Ca ions (66 percent) and has a mean n of 1.482 (R. A. Sheppard, written communication, 1971). The plot shows that n is not a sensitive indicator of either cation content or Si/Al ratio. Nevertheless it appears that a mean $n < 1.482$ implies dominantly Na–K ions and a value > 1.494 implies dominantly Ca ions. Similar implications can be made with respect to Si/Al ratios and mean n.

Figure 3 should be used with caution because some compositions have not yet been reported. For example, the upper mean n limit for clinoptilolites will probably have to be raised when a clinoptilolite–Ca is described. The lower mean n limit for Si–rich heulandites is probably close to the value shown ($n = 1.487$) as the sample defining this limit is a Na–rich specimen (sample 6). The lower mean n limit for heulandites may be close to the value shown ($n = 1.494$) as this specimen is K–rich (Alietti, 1967).

Optical orientation

Slawson (1925) recorded a rotation of the optic axial plane and change in $2V$ of heulandite when heated. In Slawson's paper it is

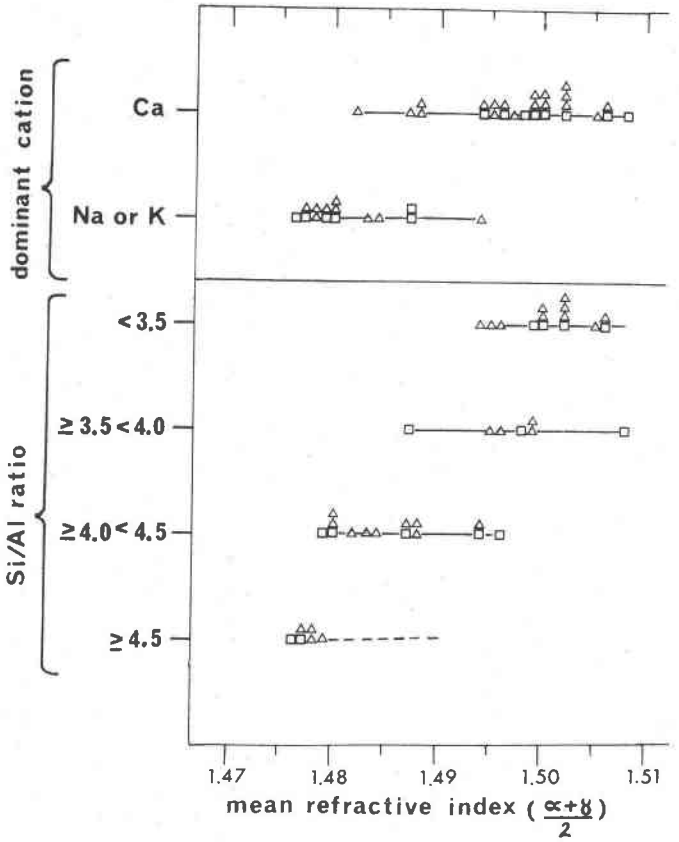

FIG. 3. Plot of Si/Al ratio and dominant exchangeable cation against mean refractive index of 41 heulandite group zeolites. Squares are data from Table 1. Triangles are data from other sources. Dashed line represents possible indices of refraction for clinoptilolite (Ca).

implied that with heating the α and β vibration directions remain parallel to the a–c crystallographic plane, which means that heulandite would remain length fast in this direction. Gilbert and McAndrews (1948) reported on a heulandite–clinoptilolite zeolite (probably Si-poor clinoptilolite or clinoptilolite as the mean index of refraction = 1.480) which was length fast when unheated but changed to length slow when mounted in Canada balsam. They also tested two established heulandites which were length fast irrespective of the mounting medium, in agreement with Slawson's data.

When samples 6 through 15 are examined in thin section prepared with Lakeside 70 (*i.e.*, thin sections heated to 100–120°C for 15–40

secs before applying cover slip) the crystals are length slow. The remaining samples of Table 1 are length fast when prepared in Lakeside 70. In thin sections which are mounted with araldite mounting medium (*i.e.*, cold) all the samples of Table 1 are length fast except samples 12 and 14.

The only chemical similarity between the samples which are length slow when heated is that all have a Si/Al ratio $\geq$3.57. This conclusion was confirmed with numerous other samples. Using this test, I was able to select the more clinoptilolite–like specimens from a large suite of tuffs altered to heulandite group zeolites from the Southland Syncline, New Zealand. The group of samples which have length slow crystals when prepared with Lakeside 70 were later shown to have Si/Al ratios greater than 3.57 (most around 3.80–4.10) by electron microprobe analyses. Samples of Na– and K–rich clinoptilolites (Si/Al 4.75 and 5.00, respectively) described by Minato and Utada (1970) and the large clinoptilolite crystals (Si/Al = 5.0–5.2) described by Wise *et al.* (1969) were also tested. All of these samples were length slow when the crushed mineral was dispersed in molten Lakeside 70, confirming the previous observations. Sheppard and Gude (1969) also reported that some large zoned clinoptilolite crystals from the Barstow Formation, California, have varying optical orientations within a crystal. The cores are length slow, but the rims are length fast. Subsequent microprobe analyses revealed that the rims contain 2.9–3.5 weight percent less SiO_2 than the core.

In summary, optical orientation after heating appears to be related to Si/Al ratio. Present data indicate that zeolites with Si/Al ratios $\geq$3.57 are length slow when prepared in Lakeside 70, but those with Si/Al ratios $\leq$3.52 are length fast.

Unit Cell Determinations

Unit cell dimensions were determined from diffractograms indexed on the assumption that heulandite and clinoptilolite have essentially identical structures and the same space group. Merkle and Slaughter (1968) determined the heulandite space group as *Cm*. Hey and Bannister (1934) had previously concluded from single–crystal photographs that heulandite and clinoptilolite are identical in structure, and this observation is verified by the close similarity of diffractograms of these minerals when the zeolites are of similar crystallite size. Reflections having similar spacings and intensities were therefore indexed the same for all members of the series. Computer refinement confirms that most clinoptilolite and heulandite reflections recorded in diffractograms can be satisfactorily indexed.

Alternate settings of the monoclinic unit cell have been used by different authors: body–centered $\beta = 91°26'$ by Wyart (1933), *c*–face centered $\beta = 113°59'$ by Shepard and Starkey (1966), and *c*–face centered $\beta = 116°20'$ by

Strunz and Tennyson (1956) and Merkle and Slaughter (1968). The latter setting is here adopted although the setting of Wyart (1933) gives a closer approach to orthogonal axes.

Quartz was used as an internal standard for all samples. Two portions of each powdered specimen were prepared on glass slides using ethyl alcohol as a dispersing agent. The following diffractometer settings were used:

Radiation:	Cukα	Time constant:	4
Filter:	Ni	Rate meter:	8
Scan speed:	$\frac{1}{2}$°/minute	Chart speed:	400mm/hour
Slits:	1°–0.2mm–1°	Instrument:	Phillips

A specially constructed scaled measuring bar with a horizontal sliding plate was clamped over the diffractograms. Peak positions were generally selected at 2/3 peak height and $\frac{1}{2}$ peak width. Conversions of peak positions to degrees 2θ were based on an average of the $10\bar{1}1$ and $10\bar{1}0$ quartz reflections at 26.662° 2θ and 20.876° 2θ, respectively. Peak positions were taken as the average from the two diffractograms. The average precision of measured peak positions is $\pm$ 0.006° 2θ.

Refinement of cell dimensions

Two computer programs were used for refining unit cell parameters: DSPACE (written by P. B. Read) and INDCER (Evans *et al.*, 1963). The former program generates all possible d spacings given extinction conditions and unit cell dimensions, and the latter program is used for refinement of cell dimensions.

The refined cell dimensions are based on reflections which occur at $<31°$ 2θ. It is necessary to base the refinement on these low-angle reflections because with higher angle reflections, attempts to index all diffractograms identically becomes increasingly difficult. In addition, the sharp reflections for heulandite and clinoptilolite diffractograms are at $<33°$ 2θ. Some accuracy is necessarily sacrificed by excluding the higher angle reflections.

The DSPACE program generates approximately 60 possible reflections at $<33°$ 2θ for CuK_α radiation. Some of these are not recorded by the diffractometer, and others are eliminated by comparison of intensities on single-crystal Weissenberg photos. Some peaks are composite.

For each sample, cell dimensions were calculated initially from a few reflections which lacked ambiguities. A new set of possible reflections were then generated using the DSPACE program allowing more of the observed reflections to be indexed. Unit cell dimension were then refined again with the INDCER program. By this procedure all reflections at $<35°$ 2θ were satisfactorily indexed. In order that the refined cell dimensions for all samples could be compared, only identically indexed reflections were accepted for the final calculation.

Results

Computer-refined cell dimensions for the 16 heulandite and clinoptilolite samples are shown in Table 1. Table 2 gives the indices used in the unit cell refinement and the range of d spacings measured for the 16 specimens. Figure 4 shows typical heulandite and clinoptilolite patterns with the appropriate indexing.

The unit cell dimensions of the heulandite and clinoptilolite samples are 17.623–17.725Å for a, 17.864–18.054Å for b, 7.392–7.431Å for

TABLE 2: Summary of diffraction data used for cell refinement of 16 heulandite group minerals.

(hkl)	n[a]	Maximum d obs (Å)	Minimum d obs (Å)	Maximum °2θ (Cukα)	Minimum °2θ (Cukα)	Intensity Range (I/I°)	Average (I/I°)
(020)	16	9.0536	8.9702	9.860	9.769	57-100	79
(200)	16	7.9351	7.8942	11.208	11.150	20-55	32
(20$\bar{1}$)	16	6.8077	6.7518	13.112	13.004	10-25	18
(001)	16	6.6658	6.6256	13.363	13.282	7-17	13
(220)	6	5.9319	5.9252	14.934	14.882	5-20	7
(130)	1	5.5817		15.887		5	
(31$\bar{1}$)	16	5.2621	5.2184	16.990	16.848	10-37	21
(111)	16	5.1241	5.1045	17.372	17.305	22-40	28
(13$\bar{1}$)	16	4.6785	4.6399	19.127	18.968	22-67	31
(040)	3	4.5131	4.4668	19.876	19.831	5-15	8
(40$\bar{1}$)	15	4.3669	4.3445	20.441	20.335	7-15	12
(221)	13	3.8483	3.8347	23.194	23.111	10-17	12
(20$\bar{2}$)	12	3.7128	3.6991	24.057	23.967	10-15	12
(31$\bar{2}$)	16	3.5663	3.5480	25.098	24.967	10-20	18
(22$\bar{2}$)	16	3.4327	3.4157	26.087	25.955	17-47	37
(311)[b]	16	3.4045	3.3835	26.339	26.174	20-42	27
(42$\bar{2}$)	16	3.1808	3.1645	28.199	28.051	17-42	35
(44$\bar{1}$)	16	3.1360	3.1187	28.621	28.460	20-30	25
(13$\bar{2}$)	16	3.0842	3.0719	29.067	28.949	10-22	17
(151)[c]	16	2.9892	2.9659	30.130	29.889	45-80	57

[a] number of samples in which this reflection was indexed.

[b] (40$\bar{2}$) may have contributed to this reflection in some samples.

[c] (350) may have contributed to this reflection in some samples.

c, and 116°15.3–116°25.9′ for β. Unit cell volume is 2,093–2,124Å^3. The cell dimensions of the Nova Scotia heulandite (sample 1) are comparable to those for a heulandite from Wallis, Switzerland of a = 17.73, b = 17.82, c = 7.43Å, and β = 116°20′ (Merkle and Slaughter, 1968). Heulandites have larger a, c, and β dimensions than clinoptilolites.

Correlation of unit cell dimensions with mineral composition

The a, c, and β dimension of heulandites and clinoptilolites show a positive correlation with cell chemistry, as does the cross sectional area of the ac plane (area = $a \times c \times \sin [180° - \beta]$). Figures 5a and 5b show an increase in ac plane area with an increase in divalent cations and with an increase in Al, respectively. The standard error of estimate of the ions on the ac plane area in Figures 5a and 5b is 0.43 and 0.42 ions/unit cell, respectively. If the ac plane area is plotted

against $Al^{+}(\Sigma\ Ca + Mg + Sr + Ba)$, the correlation is better than in either Figure 5a or 5b. The significance of the latter correlation is unknown, but it is probably because some points (*e.g.*, sample 9) fall on opposite sides of the "best fit" line in Figures 5a and 5b.

A plot of Al vs Σ Ca + Mg + Sr + Ba demonstrates that the two

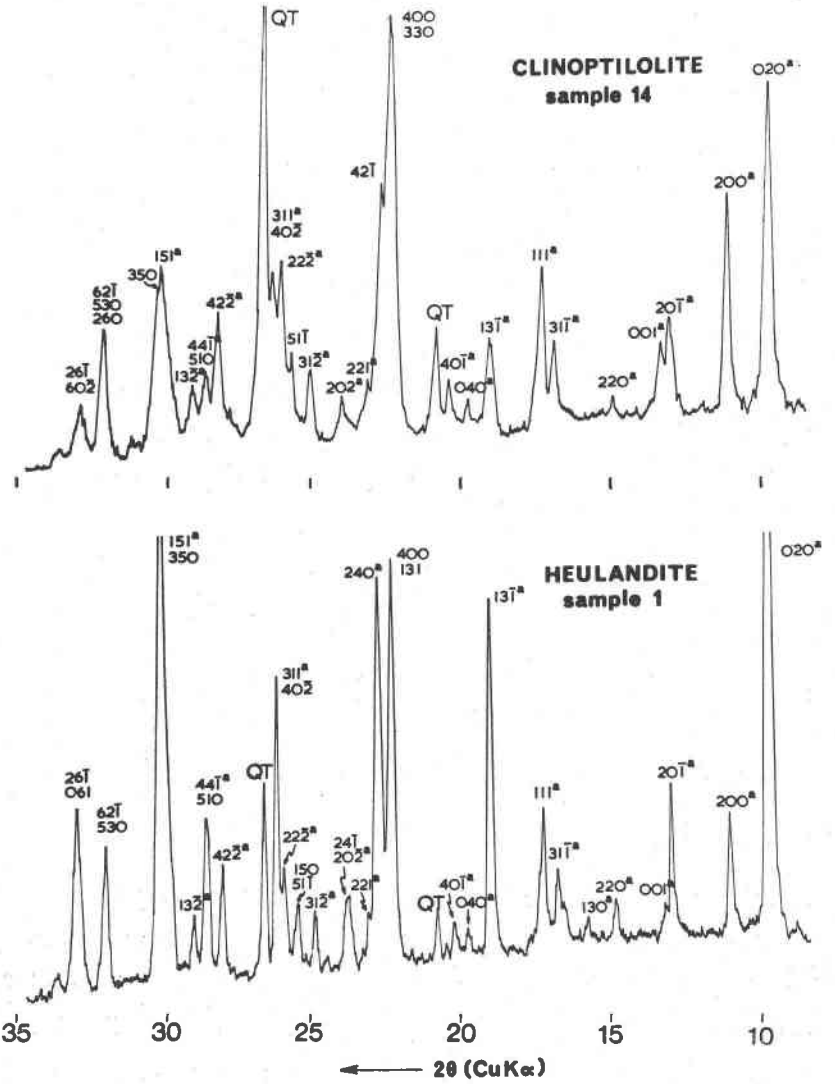

FIG. 4. X-ray diffractograms of heulandite and clinoptilolite with indexed reflections. a = indices used for cell refinement, QT = quartz.

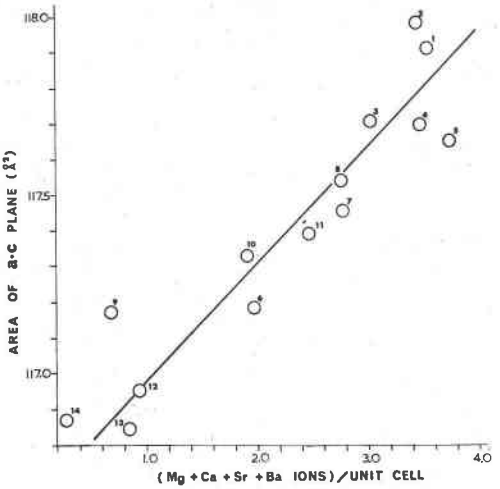

FIG. 5a. Plot of area of *ac* plane [area = $a \times c \times \sin(180° - \beta)$] against sum of exchangeable divalent cations (sum = Mg + Ca + Sr + Ba). Numbers refer to samples in Table 1.

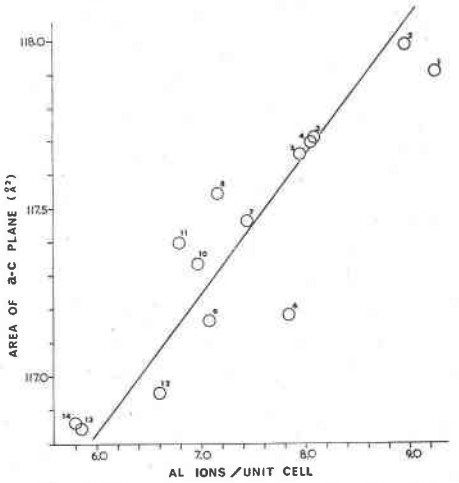

FIG. 5b. Plot of area of *ac* plane [area = $a \times c \times \sin(180° - \beta)$] against Al ions/unit cell. Numbers refer to samples in Table 1.

variables are not entirely independent. Therefore, it is difficult to interpret to what degree either Al or Σ Ca + Mg + Sr + Ba influences the area of the *ac* plane. Nevertheless, the observed relationship between Al and area of the *ac* plane is predictable from the Si–O and Al–O bond lengths determined by Merkle and Slaughter (1968). They

reported that the Si–O bond is 1.62Å, and where the tetrahedral site is partially occupied by Al the bond length increases to about 1.66Å. This explains the increase in *ac* plane area with increased Al substitution.

The correlation between divalent cations and *ac* plane area may be a result of the larger amount of water associated with these cations than with monovalent cations, which might increase the area of the *ac* plane. Alternatively, the correlation may be apparent because high Σ Ca + Mg + Ba + Sr values tend to be associated with high Al values.

The variations in the *ac* plane can be detected in the $(40\bar{1})$ reflection. Such (*h*0*l*) reflections are unaffected by the relatively large variations in the *b* cell dimension, which affects all (*hkl*) reflections. However, the shift of the $(40\bar{1})$ reflection is only 0.11° 2θ and is not convenient for quick differentiation of heulandite from clinoptilolite.

The *b* cell dimension shows a greater variation than either *a* or *c* in heulandite and clinoptilolite, but the *b* dimension cannot be correlated with either divalent cations (Σ Ca + Mg + Sr + Ba) or Al content. This suggests that an ion unique to neither heulandite or clinoptilolite may be responsible for these variations. Shepard and Starkey (1966) reported that cell size increases when K enters either heulandite or clinoptilolite. Coombs (1958) noted larger *d* spacings in clinoptilolite than in heulandite which he attributed to the presumed higher K content of the former. Figure 6a is a plot of *b* cell edge vs K content and demonstrates that the increase in *b* cell edge is not due to K substitution. Figure 6b is a plot of *b* cell edge vs Mg content and shows that this ion tends to increase the *b* cell edge.

The reason for the relationship between *b* and Mg content is unclear. From a size consideration, the small ionic radius of the Mg ion (0.65Å) compared with Ca(0.99Å), and K (1.33Å) ions would not appear to preferentially increase the *b* cell edge. However, the *hydrated radius* of the Mg ion may be large compared with hydrated Ca, Na, and K ions. Breck (1964) reported that the hydrated radius of the Na ion is actually slightly larger than that of a hydrated K ion, and it has already been demonstrated in this paper that more H_2O molecules are associated with divalent cations than with monovalent cations. Therefore, an increase in *b* cell edge could result from substitution of hydrated Mg ions, which may have relatively large radii.

Heulandite *B*

The term heulandite *B* (Mumpton, 1960) refers to the contracted

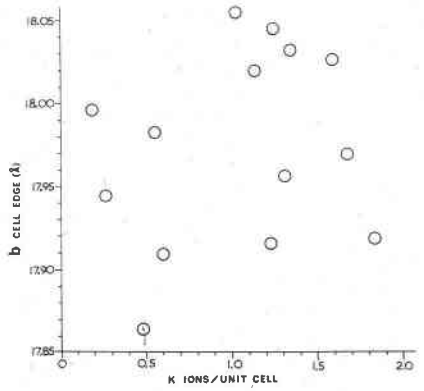

FIG. 6a. Plot of b cell edge against K ions/unit cell. Data from Table 1.

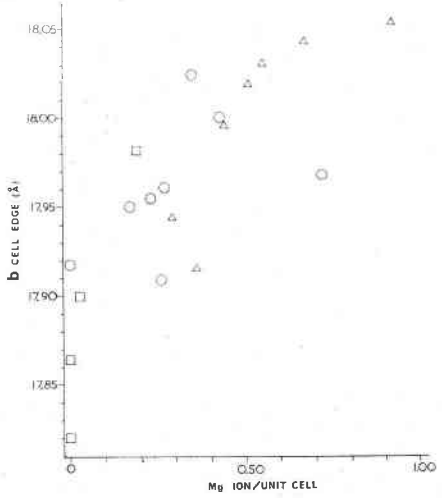

FIG. 6b. Plot of b cell edge against Mg ion/unit cell. Data from Table 1 and from Hay (1963), Ogawa (1967), and Merkle and Slaughter (1968). □ = wet chemical analysis of crystals from an amygdale. ○ = wet chemical analysis of zeolite separated from vitric tuff. △ = EMA analysis of zeolite in vitric tuff.

state of heulandite due to dehydration (Wyart, 1933). The contraction can be induced by heating or by suitable dehydrating conditions. An X–ray powder diffraction study of heulandite "B" has been made on the Nova Scotia heulandite (sample 1) to compare the behavior of a well–defined heulandite with that of the other specimens described in this report.

Ground portions of sample 1 were dispersed on glass slides which were then placed in a preheated laboratory oven (temperature monitored with a calibrated glass thermometer and chromel–alumel thermocouples). After heating and cooling for specified periods the slides were X-rayed using the previously described diffractometer settings but with a scan speed of 1°/min. and chart speed of 800 mm/hr. After measuring *d*-spacings, least squares refined cell parameters were obtained from a computer program written by Cox and Stewart (1967) and modified by P. B. Read. A new slide was prepared for each thermal test to avoid reheating of samples.

It should be noted that the structural states which result from these and other heating experiments which I have conducted were determined at room temperature after heating and are not inferred to be the state which is present at a particular high temperature. Wyart (1933), Ogawa (1967), and Breger *et al.* (1970) have determined structural states of heulandite at high temperatures.

Results

Changes in the (020) reflection of heulandite after heating for various periods at 262°C and cooling at 18–20°C for 1 hour at 1 atm are shown graphically in Figure 7. Unit cell dimension of the contracted heulandite phases are shown in Table 3. Conclusions which can be drawn from these experiments and from other thermal tests are as follows:

1. Heating of heulandite results in a contraction of *a*, *b*, and *c* cell dimensions and an increase in the β angle (see Table 3). The maximum reduction in unit cell volume is about 310Å^3.

2. After heating, two phases coexist, each of which has contracted spacing relative to unheated heulandite (*e.g.*, Fig. 7). The more contracted phase, which is hereafter called phase *B* following Hay (1963), Breger *et al.* (1970) and Alietti (1972), has a *d* (020) of 8.25–8.35Å. Following Alietti (1972) the less contracted phase is hereafter called phase *I*, and has a *d* (020) of 8.73–8.87Å.

Above a critical temperature of 202 ± 3°C but below the temperature at which the mineral becomes amorphous to X-rays (450°C after heating for 15 hours), the proportion of phase *B* relative to phase *I* increases with increased temperature at a fixed heating period or with increased heating time at a fixed temperature.

Cooling of the sample results in a reversal of this process with phase *I* gradually increasing in amount relative to phase *B*. For example, in a sample which has been heated for 2 hours at 233°C ± 3°

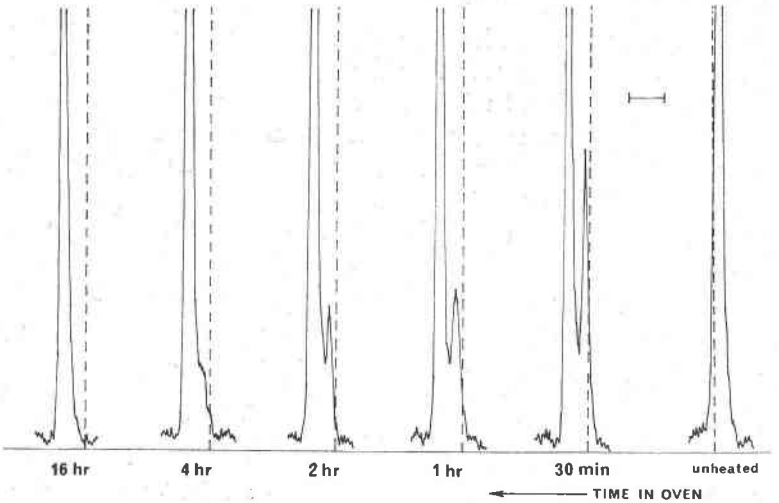

FIG. 7. Change in (020) reflection of heulandite (sample 1) after heating 5 specimens for various times at 262°C ± 3° and cooling for 1 hour. Dashed line = 10°2θ (CuKα). Horizontal bar represents a distance of 1°2θ.

and then placed on the diffractometer, the relative intensity of phase *B* progressively increases from 27 to 68 while that of phase *I* progressively decreases from 73 to 32 during a 40-minute cooling period.

3. Phases *I* and *B* do not have fixed cell parameters, but each shows a slight but generally progressive contraction with increased heating time (see Table 3). The progressive contraction of phases *I* and *B* is exemplified by the (020) reflection which gradually shifts from 8.784Å

TABLE 3: Unit cell dimensions of heulandite (sample 1) after heating at 262°C ± 3° for various times and cooling for 1 hour at 18-20°C, 1 atm. pressure.

Heating time	Percent of phase present ±			a(Å)	b(Å)	c(Å)	β (degrees)	Volume (Å^3)
	"A"	"I"	"B"					
No heating	100	0	0	17.722±.0004	17.865±.0002	7.423±.0001	116.435°±.002	2,104.38
30 min	0	35	65	"I" 17.440±.010 "B" 16.999±.072	17.529±.007 16.483±.034	7.394±.006 7.287±.024	116.61±.0001 117.10±.0005	2,021.05 1,817.49
1 hour	0	20	80	"I" 17.475±.010 "B" 17.070±.022	16.514±.006 16.505±.018	7.384±.007 7.290±.013	116.33±.0001 117.31±.0003	2,025.39 1,825.01
2 hours	0	20	80	"I" "B" 17.012±.014	16.512±.012	7.295±.009	117.22±.0002	1,822.28
4 hours	0	10	90	"I" "B" 16.951±.047	16.481±.023	7.264±.016	117.17±.0004	1,805.33
16 hours	0	0	100	"I" "B" 16.921±.016	16.417±.008	7.246±.005	117.48±.0001	1,785.89

[a] estimated from relative intensities of (020) reflection.

to 8.727Å and 8.345Å to 8.255Å, respectively, for the conditions shown in Table 3. For untreated heulandite the (020) reflection at 20–25°C is at 8.970Å. Comparing refined cell dimensions from certain heated intervals, for example 30 minutes against 1 hour heating times, one observes a slight increase in some cell dimensions. This expansion is believed to be only an apparent increase due to the large standard errors of these cell refinements.

Previous investigations implied that X–ray reflections from the contracted phases of heulandite occur at fixed *d*-spacings, *e.g.*, Shepard (1961), and Hay (1963) rather than over small ranges of *d*-spacings. Breger *et al.* (1970) noted a gradual increase in 2θ from 9.9 to 10.16° (CuKα radiation) corresponding to phase *I* of this paper.

4. A general reduction in peak intensity occurs with longer heating times and/or higher temperatures. An exception to this generalization occurs with the appearance of phase *B*, where two reflections become more intense. The *d*–spacings of these reflections are 5.182–5.215Å and 3.621–3.648Å. The DSPACE computer program indicates that these two reflections should be indexed as $(22\bar{1}, 130)$ and (240), respectively. Ogawa (1967) reported abrupt intensity increases for two reflections with similar *d*–spacings to those given above, which he indexed as (130) and (240). Ogawa also noticed an increase in relative intensity of the (020) reflection—a phenomenon not observed by me.

5. Using a fixed heating time of 15–16 hours with a short cooling period (less than 1 minute) the shift to phase *I*, as defined above, occurs at 202°C ± 3°. Under these conditions a weak reflection corresponding to phase *B* also forms (relative proportion of phase *I* to *B* is about 8:1). Apparently phase *I* can be formed at room temperature by placing the heulandite in a vacuum. Ogawa (1967) reported a change in (020) spacing from 9.03Å at 1 atm. to 8.75Å (phase *I*) in a vacuum.

6. In general, higher temperatures and/or longer heating times result in more rapid and permanent phase changes, stronger development of phase *B* and in a greater degree of destruction.

The above conclusions differ from those of Breger *et al.* (1970) who reported the first occurrence of the heulandite *B* phase near 255°C while heating a sample of heulandite from Berufjord, Iceland on a heating stage. The Cape Blomidon heulandite shows a development of this phase at temperatures as low as 202°C after heating for 16 hours. These differences probably reflect the different heating and cooling processes and possible differences in sample composition.

Breger *et al.* (1970) found no phase changes when their sample was continuously heated at the same temperature on a heating stage. For samples which I have tested, above the critical temperature and heating and cooling at 1 atm, the rate of phase change can be closely related to heating time (*e.g.*, Fig. 7). Under the experimental conditions described here, both heating time and cooling time must be carefully controlled for reproducible results, as also noted by Alietti (1972).

Cause of structural contraction

The structural collapse in heulandite is generally attributed to dehydration, *e.g.*, Slawson (1925); Wyart (1933); Breger, *et al.* (1970). However, Breger *et al.* (1970) showed that clinoptilolite loses a similar amount of water in the same temperature range as heulandite. Heulandite–Ca undergoes a structural contraction and clinoptilolite–Na, K does not; therefore, the heulandite structural contraction would not appear to be due to water loss in itself. Shepard and Starkey (1966) demonstrated that a clinoptilolite in which Ca is substituted for Na–K shows a similar structural contraction to heulandite. They also reported that substitution of K in a heulandite results in greater thermal stability. Shepard and Starkey's work demonstrated the dependence of structural contraction on the type of exchangeable cation.

Merkle and Slaughter's (1968) structural analyses of a heulandite showed that 5 water molecules are co-ordinated about each Ca ion. Furthermore their investigation showed that two of the five water molecules are more closely bonded than the other three. Ogawa (1967) indicated that in a heulandite which he studied the contracted phase (Phase *I*) which forms in a vacuum results from the loss of 10.18 wt. percent H_2O or about 3/5 of the initial total water content (16.20 wt. percent). Breger *et al.* (1970) found that a thermally induced lattice contraction appeared between 25°C and 180°C (phase *I* of this study) in their sample and they suggest that "this was probably related to the loss of loosely held water . . .", *i.e.*, the outer three water molecules. Furthermore they have suggested that transition to phase *B* occurs after partial removal of the inner two water molecules.

The removal of water from Ca ions in the heulandite structure may cause these ions to shift position in the structure and hence cause structural distortion. Removal of the outer three water molecules may result in only a slight shift of position with a slight contraction resulting (phase *I*). Partial removal of the inner two water molecules may result in more drastic shift of Ca–ion positions and a relatively large contraction results: (phase *B*). Marked changes in atomic position are suggested by

the marked increase in relative intensity of the ($22\bar{1}$, 130) and (240) reflections in phase *B*.

A similar phenomenon occurs in other zeolites. The cation position in chabazite (Breck, 1964) and in the synthetic zeolite Zk–5 (Meier, 1968) is supposedly a function of dehydration state. In the case of chabazite, structural distortion is noted during dehydration as the Ca ion changes position (Breck 1964). The contraction in the Ca zeolite laumontite (Coombs, 1952) when dehydrated to leonhardite may also result from a similar shift in atomic position.

The reported structural changes in a dehydrated Ca–clinoptilolite (Shepard and Starkey, 1966) support the conclusion that the Ca ion is of major importance in causing these phase changes. However, Shepard and Starkey reported that even with almost complete Ca substitution in clinoptilolite, the structural contraction is 75°C higher than the transformation in heulandite–Ca. The clinoptilolite framework contains more Si–O bonds than heulandite, which presumably can strengthen the framework. As will be subsequently shown, thermal stability data from the New Zealand samples support this conclusion.

Thermal Stability

Thermal stability is used by many investigators as a rapid method to distinguish between heulandite–clinoptilolite. The test, proposed by Mumpton (1960), involves heating the sample at 450°C overnight and then X–raying. Heulandite is supposedly destroyed (X–ray amorphous), but clinoptilolite remains unchanged. Several workers have reported members of the group which show "intermediate" thermal stability (*e.g.*, Hay, 1963; Shepard, 1961; Shumenko, 1964; *Brown et al.*, 1969; Minato and Utada, 1970; and Alietti, 1972).

Brown *et al.*, Minato and Utada, and Alietti have shown that minerals with intermediate thermal stability have a composition intermediate to most samples of heulandite–Ca and clinoptilolite–Na or K. I attempted to establish whether or not zeolites with slightly different compositions can be distinguished by thermal stability tests.

Samples were prepared on glass slides or silicon plates prior to heat treatment so that they could be X–rayed immediately after the cooling period. This procedure prevented rehydration which could have occurred due to X–ray slide preparation, and it had the added advantage of standardizing the volume of powder heated. A new sample was prepared for each temperature investigated as heating, cooling, and reheating of the same sample results in progressively

lower temperatures at which phase changes take place (see Breger *et al.*, 1970).

The ovens were preheated to the desired temperature for all experiments. Temperature was monitored with chromel–alumel thermocouples when greater than 350°C, and with a calibrated glass thermometer when less than 350°C. After heating, the samples were cooled in a temperature controlled room (18–22°C).

Results

Results of the thermal stability experiments are summarized in Table 4. In general heat treatment causes either a *d*–spacing contraction accompanied by X–ray intensity reduction or by an intensity reduction without changes in *d*–spacings.

The results shown in Table 4 indicate that the thermal stability of these heulandites and clinoptilolites can be classified into one of three groups:

Group 1: (a) Characterized by complete destruction at 450°C for 15 hours.
(b) Formation of the phases *I* and *B* contracted state. Phase *I* appeared at temperatures of 212–250°C, *e.g.*, samples 1–5, and 16. Phase *B* contracted state formed in all samples of this group, but the phase is not shown on Table 4.

Group 2: (a) Characterized by partial destruction at 450°C for 15 hours. A portion of the original (020) reflection persists at temperatures greater than 450°C.
(b) Formation of the phases *I* and *B* contracted state. Phase *I* appeared at temperatures equal to or greater than 255°C, *e.g.*, samples 6 through 8, 10 and 11.

Group 3: (a) Characterized by general stability at 450°C for 15 hours.
(b) *d*–spacing unchanged at all temperatures. However, some destruction was indicated by a reduction in intensity in the 450–650°C range, *e.g.*, samples 9 and 12 through 15.

The results shown above are in close agreement with the thermal stability data of Alietti (1972). By heating at 550°C for 12 hours, Alietti recognized 3 main types of thermal stability in heulandite group minerals and demonstrated that the difference of thermal behavior is due both to different Si/Al ratios and divalent cation contents of the minerals. Minerals of Group 1 thermal stability plot into the

TABLE 4: Thermal stability of the 16 heulandite group minerals from Table 1.

	Temperature required for appearance of phase "I"[a]	Relative intensities of (020) reflections after heating[b]								
		450°C			550°C			650°C		
		A	I	B	A	I	B	A	I	B
1	213°C	destroyed								
2	212°C	destroyed								
3	248°C	destroyed								
4	248°C	destroyed								
5	250°C	destroyed								
6	255°C	21		46	38		<5	40		
7	290°C	20		6	16		5	12	5	<5
8	295°C	22			15	5	<5	12	5	<5
9	n.d.	66			60			50		
10	>300°C	16		14	n.d.			n.d.		
11	312°C	26	10	5	16		<5	14	8	<5
12	n.d.	100			84			80		
13	n.d.	100			100			66		
14	n.d.	100			100			84		
15	n.d.	90			90			74		
16	240°C	destroyed								

[a] Samples heated for 2 hours and cooled for 1 hour. Phase "I" appeared ±3°C of temperature stated.

[b] Samples heated for 15 hours and cooled less than 1 hour. Initial (020) intensity of phase was 100. (020) spacings of phases:

A = initial phase = 8.97-9.05Å
I = phase I = 8.73-8.87Å
B = phase B = 8.30-8.35Å

composition field of "heulandite type 1" in the mole plot Si_9O_{18}–$Ca_{4.5}Al_9O_{18}$–$Na,K_9Al_9O_{18}$ shown by Alietti. Similarly, Group 2[1] and 3 types plot in composition fields of "heulandite type 2" and "clinoptilolite" shown by Alietti.

The new data shown here allow the contraction phenomena to be interpreted more fully. Specifically, samples of Group 1 have a SD[2] value greater than 2.94, those of Group 2 have a SD value of 1.87–2.90, and those of Group 3 have a SD value less than 1.00. The data indicate that when the sum of the divalent cations exceeds 1.87, the

[1] Sample 6 plots just inside of Alietti's "clinoptilolite" composition field but does not conflict with the data given.

[2] SD = sum of divalent cations = $(Ca^{2+} + Mg^{2+} + Sr^{2+} + Ba^{2+})$

contracted phases form. Shepard and Starkey (1966) documented the effect of exchanged cations on thermal stability of heulandite and clinoptilolite. They reported that a clinoptilolite–Ca contracts upon heating whereas a heulandite–K does not. Anomalously, Na–treated heulandite and clinoptilolite contracted upon heating. Shepard and Starkey, however, reported that the heulandite had recrystallized during the exchange experiments.

Although the type of cations may control whether or not contraction will occur, thermal stability also correlates with Si/Al ratios. Figure 8 shows a plot of temperatures at which contraction first occurs, with 2 hour heating and 1 hour cooling against Si/Al ratio for samples of Groups 1 and 2. The plot demonstrates that the initial temperature for contraction is related to Si/Al ratio. Higher Si/Al ratios progressively strengthen the framework against contraction, but the relatively high proportion of divalent cations in the samples eventually permits contraction. The higher Si/Al ratios of minerals in Group 2 (Si/Al $\geq$ 3.57) compared with those in Group 1 (Si/Al $\leq$ 3.52) may have caused the persistence of part of the original phase observed after heat treatment.

The samples of Group 2 are of particular interest because they have thermal stabilities intermediate between most heulandites and clinoptilolites. These specimens show a persistence of the original (020) reflection even though the majority of the specimen is destroyed after heating at 450–650°C. In addition, the intensity of the persisting

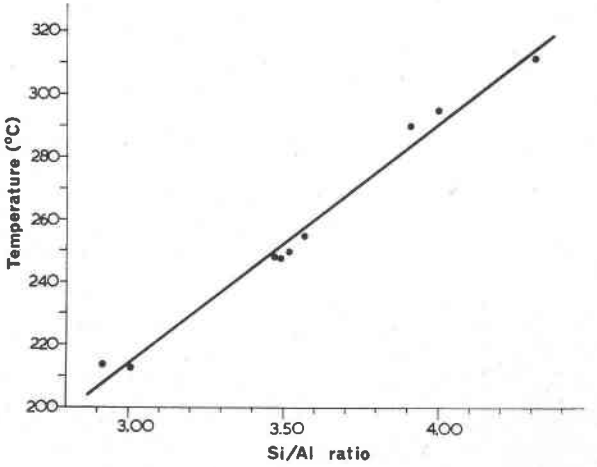

FIG. 8. Plot of temperature required for appearance of phase *I* against Si/Al ratio of sample. Data from Table 1 and Table 4.

phase becomes weaker at higher temperatures, sample 6 being the exception (see Table 4). A similar phenomenon was reported by Hay (1963) for a heulandite group mineral from Oregon and by Alietti (1972). The thermal stability of Group 2 could be attributed to a mixture of clinoptilolite and heulandite; however, the minerals have a relatively uniform refractive index and no discernible zoning was found with an electron microprobe (10 μm beam diameter). In addition the higher temperatures required to induce phase changes (Fig. 8) do not indicate a mixture of heulandite and clinoptilolite. Therefore, it is concluded that the thermal stability of Group 2 is a characteristic of the "intermediate" compositions (*cf.*, Alietti, 1972). Nevertheless, it is difficult to understand how a portion of the mineral can persist, while the remainder is destroyed without compositional disordering on at least a submicroscopic scale.

The samples of Group 3 show no contracted phases at any temperature (*cf.* Alietti, 1972). However, a partial breakdown of structure occurs in the 450–650°C temperature range. Sample 9 shows the greatest degree of destruction in this temperature range, possibly due to its relatively low Si/Al ratio (4.12).

Estimating composition of heulandite group minerals

The composition of a heulandite group mineral can be estimated from optical properties, unit cell dimensions, and thermal stability. Two examples of the procedure are given below using samples 15 and 16.

Sample 15. The mineral is length slow which indicates a Si/Al ratio $\geq$ 3.57 (see Table 1). A mean index of refraction of 1.484 indicates a Si/Al ratio $\geq$ 4.00 (see Fig. 3). The *b* cell dimension of sample 15 is 17.90Å and indicates a very low Mg content, probably less than 0.20 ion/unit cell (see Fig. 6b). *a*, *c*, and β parameters give an *ac* plane area equal to 117.22Å^2, a value greater than the areas determined for samples 9, 12, 13, and 14. Sample 15, therefore has more divalent cations than the latter specimens (see Fig. 5a) and/or it has more Al (see Fig. 5b), *i.e.*, a lower Si/Al ratio. Thermal stability indicates that the SD value is less than 1.00 indicating predominantly monovalent cations similar to samples 12, 13, and 14. Re-examination of the interpretation from unit cell data indicates that sample 15 probably has a lower Si/Al ratio than samples 12, 13, and 14 and is probably most similar to sample 9. Therefore, the Si/Al ratio of sample 15 is estimated between 4.00 and 4.31. This sample can tentatively be classified as *Si-poor clinoptilolite–Na or –K.*

Sample 16. The mineral is length fast which indicates a Si/Al ratio

$\leq$ 3.52 (see Table 1). A mean refractive index of 1.500 indicates a Si/Al ratio less than 4.00 and predominantly Ca ions. The *b* cell dimension is 18.02Å and indicates a unit cell Mg content of about 0.30 to 0.50 ion/unit cell (see Fig. 6b). *a*, *c*, and β parameters give an *ac* plane area of 117.88Å which is a lower value than that for sample 1 but greater than that of sample 3. This indicates that sample 16 has an intermediate divalent cation content with respect to these samples and/or intermediate Al content. As all three samples have Group 1 type thermal stability (indicating similar divalent cation contents), one might guess that sample 16 has an intermediate Al content with respect to the other two samples. This implies a Si/Al ratio of 2.94–3.47. The initial phase change occurs at 240°C (see Table 4) and indicates a Si/Al ratio between 3.2 and 3.4 (see Fig. 7). Sample 16 can tentatively be classified as a heulandite–Ca.

Acknowledgments

The author wishes to acknowledge the following individuals and organizations for samples: Dr. R. A. Sheppard of the U.S.G.S., Denver, Colorado; Dr. L. J. P. Muffler of the U.S.G.S., Menlo Park, California; Dr. W. S. Wise of the University of California, Santa Barbara, California; Dr. H. Minato of the University of Tokyo, Japan; U.S. National Museum, Washington, D.C.; and Deep Sea Drilling Project, National Science Foundation. Dr. P. B. Read of the Department of Geology, University of British Columbia, Vancouver, is thanked for assistance with single crystal photographs and computer refinement. Mr. J. M. Pillidge, University of Otago technical staff, provided excellent polished sections for EMA analysis. Permission to use the EMA analyser at the Research School of Physical Sciences, Canberra, Australia, and the assistance of Mr. N. G. Ware is gratefully acknowledged. Dr. D. S. Coombs of the University of Otago, and Dr. R. A. Sheppard critically reviewed the manuscript. Lastly the author wishes to thank Dr. D. S. Coombs for his continuous encouragement and helpful advice during the course of this investigation. The research has been supported by National Science Foundation Grant GA 754 (Coombs).

References

Alietti, A. (1967) Heulanditi e clinoptilotiti. *Mineral. Petrogr. Acta* **13**, 119–138.

——— (1972) Polymorphism, and crystal-chemistry of heulandites and clinoptilotites. *Amer. Mineral.* **57**, 1437–1451.

Ames, L. L. Jr., L. B. Sand, and S. S. Goldich (1958) A contribution on the Hector, California bentonite deposit. *Econ. Geol.* **53**, 22–37.

Breck, D. W. (1964) Crystalline molecular sieves. *J. Chem. Educ.* **41**, 678–689.

Breger, I. A., J. C. Chandler, and P. Zubovic (1970) An infrared study of water in heulandite and clinoptilolite. *Amer. Mineral.* **55**, 825–840.

Brown, G., J. A. Catt, and A. H. Weir (1969) Zeolites of the clinoptilolite–heulandite type in sediments of south-east England. *Mineral. Mag.* **37**, 480–488.

Coombs, D. S. (1952) Cell size, optical properties and chemical composition of

laumontite and leonhardite, with a note on regional occurrences in New Zealand. *Amer. Mineral.* **37**, 812–830.

——— (1958) Zeolitized tuffs from the Kuttung glacial beds near Seaham, New South Wales. *Austral. J. Sci.* **21**, 18–19.

———, A. J. Ellis, W. S. Fyfe, and A. M. Taylor (1959) The zeolite facies with comments on the interpretation of hydrothermal systems. *Geochim. Cosmochim. Acta,* **17**, 53–107.

Cox, A. A., and E. G. Steward (1967) An I.C.T. Fortran program for least-squares refinement of crystal structure cell dimensions. *Acta Crystallogr.* **23**, 1113–1114.

Deer, W. A., R. A. Howie, and J. Zussman (1963) *Rock-forming Minerals 4.* John Wiley and Sons, New York, 435p.

Evans, H. T., Jr., D. E. Appleman, and D. S. Handwerker (1963) The least squares refinement of crystal unit cells with powder diffraction data by an automatic computer indexing method. *Amer. Crystallogr. Assoc., Cambridge, Mass., Ann. Meet., Program.* (abstr.), 42–43.

Foster, M. D., (1965) Composition of zeolites of the natrolite group. *U.S. Geol. Surv. Prof. Pap.* **504–D**, 7p.

Gilbert, C. M., and M. G. McAndrews (1948) Authigenic heulandite in sandstone, Santa Cruz County, California. *J. Sed. Petrology,* **18**, 91–99.

Hey, M. H., and F. A. Bannister (1934) Studies on the zeolites. Part VII. "Clinoptilolite", a silica-rich variety of heulandite. *Mineral. Mag.* **23**, 556–559.

Hay, R. L. (1963) Stratigraphy and zeolitic diagenesis of the John Day Formation of Oregon. *Univ. Calif. Publ. Geol. Sci.* **42**, 199–262.

Honda, S., and L. J. P. Muffler (1970) Hydrothermal alteration in core from research drill Hole Y-1, Upper Geyser Basin, Yellowstone Park, Wyoming. *Amer. Mineral.* **55**, 1714–1737.

Iijima, A. (1970) Composition and origin of clinoptilolite in the Nakanosawa tuff of Rumoi, Hokkaido. *Amer. Chem. Soc., 2nd Int. Conf. Mol. Sieve Zeol., Worcester, Mass., preprints,* 540–547.

Mason, B., and L. B. Sand (1960) Clinoptilolite from Patagonia: The relationship between clinoptilolite and heulandite. *Amer. Mineral.* **45**, 341–350.

Meier, W. M. (1968) Zeolite structures. In *Molecular Sieves, 1964 Conf. of Soc. Chem. Industr., London,* p. 10–27.

Merkle, A. B., and M. Slaughter (1968) Determination and refinement of the structure of heulandite. *Amer. Mineral.* **53**, 1120–1138.

Minato, H., and M. Utada (1970) Clinoptilolite from Japan. *Amer. Chem. Soc., 2nd Int. Conf. Mol. Sieve Zeol., Worcester, Mass.,* preprints, 535–539.

Mumpton, F. A. (1960) Clinoptilolite redefined. *Amer. Mineral.* **45**, 351–369.

Ogawa, T. (1967) On the varieties of heulandite. *J. Sci. Hiroshim. Univ., Japan,* **5**, 267–285.

Pécsi-Donáth, E. (1966) On the relationship between lattice structure and "zeolite water" in gmelinite, heulandite, and scolecite. *Acta Univ. Szeged. Acta Mineral. Petrogr.* **17**, 143–158.

Piekarska, E., and A. Gawel (1954) Heulandite from Rudno (Cracow district). *Ann. Soc. Geol. Pologne* **22**, English summary, 367–373; [*Mineral. Abstr.* **12**, 484 (1955)].

Ross, C. S., and E. V. Shannon (1924) Mordenite and associated minerals from near Challis, Custer County, Idaho. *Proc. U.S. Nat. Museum,* **64**, 1–19.

Shepard, A. O. (1961) A heulandite-like mineral associated with clinoptilolite in

tuffs of Oak Springs Formation, Nevada Test Site, Nye Co., Nevada, *U.S. Geol. Surv. Prof. Pap.* **424-C**, C320–322.

———, AND H. C. STARKEY (1966) The effects of exchanged cations on the thermal behavior of heulandite and clinoptilolite. *Mineral Soc. India, IMA Vol.*, p. 156–158.

SHEPPARD, R. A., AND A. J. GUDE, 3d., (1968) Distribution and genesis of authigenic silicate minerals in tuffs of Pleistocene Lake Tecopa, Inyo County, California. *U.S. Geol. Surv. Prof. Pap.* **597**, 38 p.

——— (1969) Diagenesis of tuffs in the Barstow Formation, Mud Hills, San Bernardino County, California. *U.S. Geol. Surv. Prof. Pap.* **634**, 35 p.

SHUMENKO, S. I. (1962) Varieties of authigenic secondary heulandite in the Upper Cretaceous of the Ukraine. *Akad. Nauk. SSSR, Dokl., Earth Sci. Sec.* **144**, 1347–1350 (in Russian); (1964), **144**, 144–146 (English translation).

SLAWSON, C. B. (1925) The thermo-optical properties of heulandite. *Amer. Mineral.* **10**, 305–331.

STRUNZ, H., AND C. TENNYSON (1956) "Polymorphie" in der Gruppe der Blatterzeolithe. *Neues Jahrb. Mineral Monatash.*, 1.

WISE, W. S., W. J. NOKLEBERG, AND M. KOKINOS (1969) Clinoptilolite and ferrierite from Agoura, California. *Amer Mineral.* **54**, 887–895.

WYART, J. (1933) Recherches sur les zeolites. *Bull. Soc. Fr. Mineral. Cristallogr.* **56**, 81–187.

ZAPOROZHTSEVA, A. S. (1960) On the regional development of laumontite in Cretaceous deposits of Lena coal basin. *Akad. Nauk. SSSR. Izv., Geol. Ser. No.* **9**, 52–59.

Manuscript received, July 31, 1971; accepted for publication, May 11, 1972.